**PERIODICO di MINERALOGIA**
*established in 1930*

Dipartimento di Scienze della Terra
Sapienza Università di Roma

*An International Journal of*
Mineralogy, Crystallography, Geochemistry,
Ore Deposits, Petrology, Volcanology
and applied topics on Environment, Archaeometry and Cultural Heritage

# An insight on possible toxicity mechanism of fibrous erionite

Maria Cristina Di Carlo [1], Paolo Ballirano [1], Maria Rita Montereali [2], Raffaela Caprioli [2], Elisa Nardi [3], Alessandro Pacella [1,*]

[1] Department of Earth Sciences, Sapienza University of Rome, Piazzale Aldo Moro 5, I-00185 Rome, Italy
[2] ENEA, C.R. Casaccia via Anguillarese 301, I-00123 S. Maria di Galeria, Rome, Italy
[3] Italian Institute for Environmental Protection and Research (ISPRA), via Vitaliano Brancati 48, 00144 Rome, Italy

**ARTICLE INFO**

Submitted: May 2023
Accepted: June 2023
Available on line: July 2023

* Corresponding author:
alessandro.pacella@uniroma1.it

Doi: 10.13133/2239-1002/18097

How to cite this article:
Di Carlo M.C. et al. (2023)
Period. Mineral. 92, 191-201

**ABSTRACT**

Inhalation of erionite fibres is associated with endemic lung and pleural diseases. However, the mechanisms by which erionite exerts its toxic activity are not fully understood. Recently, it has been shown that erionite fibres are too short to undergo frustrated phagocytosis. On this basis, the role of phagocytosis in the acute toxicity of these fibres is supposed to be limited. Instead, it has been proposed that erionite, after phagocytosis, may activate a rapid cation exchange with cytosolic potassium, leading to the alteration of ion homeostasis and cellular injury. Furthermore, it has been hypothesised that engulfed erionite fibres may reduce cytosolic $Ca^{2+}$ levels and interfere with the cross-talk between the endoplasmic reticulum and mitochondria, resulting in the failure of cellular apoptosis. In this work, erionite fibres were incubated first in a solution mimicking extra-cellular lung fluid and then in another one simulating intra-cellular cytosol. Our goal was to gain further insights into the proposed mechanisms of acute cytotoxicity of erionite, in particular: i) to simulate possible $K^+$ binding by erionite through cation exchange after phagocytosis, and ii) to assess its potential absorption of cytosolic Ca. The ions released into the solutions were quantified by inductively coupled plasma optical emission spectroscopy. Pristine and incubated fibres were analysed by scanning electron microscopy equipped with an energy dispersive spectroscopy system and X-ray powder diffraction (Rietveld method). Results support the hypothesis that erionite can bind cytosolic K ions through a rapid cation exchange process, mainly with Na ions previously bound in the extra-cellular environment. However, our findings seem to rule out the ability of phagocytized erionite fibres to decrease cytosolic $Ca^{2+}$ levels and, consequently, to interfere with the endoplasmic reticulum-mitochondria cross-talk that regulates cell apoptosis.

Keywords: Fibrous erionite; X-ray Powder Diffraction; Rietveld method; cation release; cation exchange; erionite toxicity.

## INTRODUCTION

Erionite is a zeolite occurring worldwide, usually within volcanic and volcanically derived rocks, as a product of diagenesis or hydrothermal alteration (Gottardi and Galli, 1985; Coombs et al., 1998). Its average chemical formula is $K_2(Na,Ca_{0.5})_8[Al_{10}Si_{26}O_{72}]\cdot 30H_2O$ and, according to the most abundant extra-framework cation (EF), three different species are recognized as erionite-Na, erionite-K, and erionite-Ca (Coombs et al., 1998). Erionite belongs to the ABC-6 family (Gottardi and Galli, 1985) being the structure originated by the stacking along the c-axis of 6 layers of 6-membered rings

of $TO_4$ tetrahedra (T=Si, Al) following the sequence AABAAC. This sequence forms columns of cancrinite cages alternating with double 6-membered rings (D6R) and columns of erionite (23-hedron) cages formed by connecting adjacent columns via single 6-membered rings (S6R) at the level of the cancrinite cages. EF cations are hosted within the erionite cage at Ca1, Ca2, and Ca3 sites located along the axis of the cavity, whereas the cancrinite cage hosts only K ions at K1 site located in the cavity centre. An additional K2 site, situated at the centre of the 8-membered boat-shaped rings (8MR) forming the walls of the erionite cage, is present in erionite with K ions exceeding 2 apfu (Ballirano et al., 2009; Ballirano and Cametti, 2012). Moreover, six $H_2O$ sites (OW7, OW8, OW9, OW10, OW11, and OW12) are arranged around the axis of the erionite cage, providing coordination to EF cations (Ballirano et al., 2017). The unit cell of erionite contains two cancrinite cages, two D6Rs, and two erionite cages (Staples and Gard, 1959; Gard and Tait, 1973).

Inhalation of erionite fibres was unequivocally linked to several malignant mesothelioma cases in some villages of Cappadocia region (Turkey) in the 1970s (Artvinli and Baris, 1979; Baris et al., 1981, 1987). *In vivo* studies suggested that respirable-sized erionite fibres would be about 500-800 times more carcinogenic than chrysotile and 200 times more carcinogenic than crocidolite (Coffin et al., 1992). On these bases, in 1987 the International Agency for Research on Cancer classified erionite as a Group 1, i.e., agent carcinogenic to humans (IARC, 2012).

A growing attention to this mineral followed the discovery in North Dakota (USA) of more than 300 miles of unpaved roads built with gravel containing fibrous erionite (Carbone et al., 2011) and the identification of some mesothelioma cases possibly related to erionite in USA, Mexico, and Iran (Rom et al., 1983; Ilgren et al., 2008, 2015; Ortega-Guerrero et al., 2015).

Although it has been proven that erionite is carcinogenic to humans, the mechanism by which it induces cell damage is still not understood to date. Erionite appears to be, similarly to amphibole asbestos, extremely biopersistent (Pollastri et al., 2016; Gualtieri et al., 2017; Cangiotti et al., 2018; Pacella et al., 2021) and therefore may be able to exert its toxic action for decades within the human body. Erionite toxicity has been possibly related to Fe ion-exchanged and/or surface-deposited after fibre inhalation may, which generate hydroxyl radicals by Fenton chemistry (Eborn and Aust, 1995). Moreover, it was shown that erionite can vehiculate Fe in the human body since Fe-bearing nanoparticles (nano-oxides, sulphates, phyllosilicates) may be present on the fibre surface (Matassa et al., 2015; Gualtieri et al., 2016).

Recently, Di Giuseppe et al. (2022), based on a time-lapse video microscopy investigation coupled with *in vitro* test, reported that frustrated phagocytosis plays a limited role in the acute toxicity of erionite fibres due to their short length. Alternatively, these authors suggested that fibrous erionite during phagocytosis activates a quick cation exchange with ions present in the cytosol of macrophages (e.g., $Ca^{2+}$ and $K^{+}$), leading to dysregulation of ionic homeostasis, cell swelling and cell lysis. Moreover, they suggested that erionite fibres could reduce the level of cytosolic $Ca^{2+}$, thus interfering with endoplasmic reticulum-mitochondria cross-talk and causing the failure of cell apoptosis.

The goal of this work was to gain more insights into the acute cytotoxicity mechanisms of erionite. For this purpose, erionite fibres were previously incubated in a mimicked Gamble's solution (MGS) at neutral pH to reproduce the fibres' interaction with the extra-cellular lung fluid. Subsequently, the fibres were immersed in a neutral aqueous KCl solution at cytosolic $K^{+}$ concentration to simulate possible $K^{+}$ binding by erionite from the intra-cellular solution, as a result of cation exchange after phagocytosis. Moreover, fibres treated in MGS were incubated in the KCl solution with the addition of Ca ions to evaluate possible cytosolic $Ca^{2+}$ uptake by erionite. It must be pointed out that the adopted conditions, although far from mimicking a real physiological environment, provide a benchmark for interpreting the extremely complex processes that can occur *in vivo*.

Ions released in solutions were quantified by inductively coupled plasma optical emission spectroscopy (ICP-OES). Pristine and incubated fibres were analysed by scanning electron microscopy (SEM) equipped with an energy dispersive spectroscopy (EDS) system and X-ray powder diffraction (XRPD).

## MATERIALS AND METHODS

### Samples description and preparation

The sample investigated in this work was fibrous erionite from Rome, Oregon, USA (Figure 1). The raw material was enriched in erionite content following the procedure reported by Ballirano and Cametti (2015). The sample was classified as erionite-Na on the basis of the SEM-EDS analysis (Table 1).

### Incubation of erionite in MGS and KCl solution

The composition of the MGS was that adopted by Pacella et al. (2021) (NaCl 112.3 $mmolL^{-1}$ and $Na_2SO_4$ 0.556 $mmolL^{-1}$) to evaluate the dissolution and surface chemical modifications of fibrous erionite. In particular, the solution has the same molar composition of the Gamble's solution mimicking the interstitial lung fluid (Marques et al., 2011), except for Mg and Ca salts (that were substituted by Na salts) to avoid interferences with the extra-framework cations of erionite. Phosphate salts

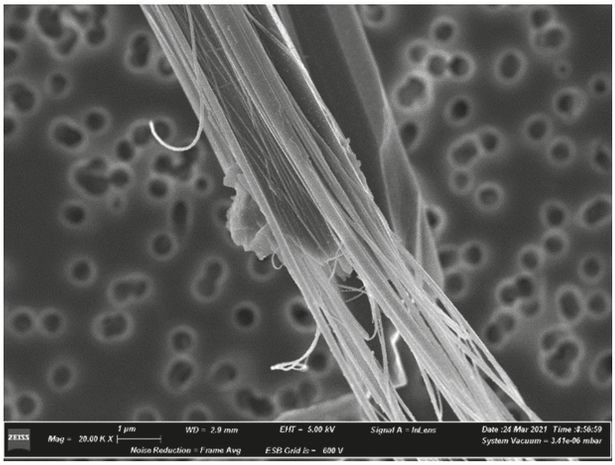


Figure 1. SEM image of erionite fibres from Oregon (USA).

were also avoided because of possible interference with Si during ICP-OES analysis.

An aliquot of 20 mg of erionite fibres were suspended for 24 hours in 40 mL of MGS solution using a Falcon™ polypropylene tube. The tubes were fully immersed in a thermostatic water-bath at a constant temperature of 37±1 °C and gently shaken. Incubation of the fibres in MGS at neutral pH was performed to reproduce the ion-exchange process of the extra-framework cations with $Na^+$ ions present in the solution (Pacella et al., 2021), possibly occurring *in vivo* when erionite is in contact with the extra-cellular lung fluid. At the end of each experiment, the solution was sampled from the tube with a syringe and filtered using a nitrocellulose membrane filter of

Table 1. SEM-EDS chemical analyses of both pristine and ion-exchanged erionite fibres. Reference data: (P17) Pacella et al. (2017b) and (P21) Pacella et al. (2021) for erionite-K samples from Rome are reported for comparison. ERI-KCl Ref 2 h correspond to the KCl-exchanged erionite-Na from Rome characterized by Pacella et al. (2017b).

| Oxides (wt%) | ERI-PRI | P17 | P21 | ERI-KCl Ref 2 h | ERI-Gamble 24 h | ERI-KCl 1 h | ERI-KCl+$CaCl_2$ 1 h | ERI-KCl+$CaCl_2$ 24h |
|---|---|---|---|---|---|---|---|---|
| $SiO_2$ | 58.40(80) | 60.06(47) | 59.47(77) | 57.35(14) | 58.98(89) | 57.00(78) | 57.78(76) | 57.11(73) |
| $Al_2O_3$ | 13.77(40) | 12.81(19) | 13.41(63) | 12.78(8) | 13.73(49) | 13.18(53) | 13.49(33) | 13.93(36) |
| $Na_2O$ | 3.26(49) | 4.03(27) | 1.73(41) | 1.46(11) | 4.73(75) | 0.36(39) | 1.11(25) | 0.81(20) |
| $K_2O$ | 4.05(42) | 4.01(42) | 4.69(43) | 9.32(13) | 3.07(22) | 9.75(65) | 7.93(38) | 8.41(106) |
| MgO | 1.12(18) | 0.59(24) | 1.10(11) | 0.59(9) | 0.70(20) | 0.78(19) | 0.83(16) | 0.82(19) |
| CaO | 0.91(26) | n.d. | 1.09(14) | - | 0.30(17) | 0.45(43) | 0.37(10) | 0.41(27) |
| FeO | n.d. | n.d. | n.d. | n.d. | n.d. | n.d. | n.d. | n.d. |
| $H_2O$* | 18.50 | 18.50 | 18.50 | 18.50 | 18.50 | 18.50 | 18.50 | 18.50 |
| Total | 100.00 | 100.00 | 100.00 | 100.00 | 100.00 | 100.02 | 100.00 | 100.00 |
| Si | 28.22(24) | 28.76(11) | 28.43(35) | 28.51(5) | 28.23(25) | 28.29(32) | 28.18(22) | 28.11(30) |
| Al | 7.78(24) | 7.24(11) | 7.57(35) | 7.49(5) | 7.77(25) | 7.71(32) | 7.82(22) | 7.89(30) |
| Na | 3.30(80) | 3.75(27) | 1.61(39) | 1.41(10) | 4.30(65) | 0.35(37) | 1.27(35) | 1.13(17) |
| K | 2.40(26) | 2.45(27) | 2.86(27) | 5.91(9) | 1.89(12) | 6.17(43) | 4.98(28) | 4.96(68) |
| Mg | 0.72(18) | 0.42(17) | 0.79(8) | 0.44(7) | 0.54(15) | 0.58(14) | 0.58(16) | 0.58(11) |
| Ca | 0.35(18) | - | 0.56(7) | - | 0.14(9) | 0.24(23) | 0.18(6) | 0.19(12) |
| Fe | - | - | - | - | - | - | - | - |
| O | 72.04(19) | 72.10(14) | 71.80(17) | 72.35(4) | 71.88(18) | 72.22(10) | 71.97(20) | 71.88(12) |
| $H_2O$ | 29.75(24) | 29.60(17) | 29.56(15) | 30.73(4) | 29.58(19) | 30.62(12) | 30.28(21) | 30.22(28) |
| E% | -0.70 | 3.10 | 5.50 | -8.60 | 3.30 | -5.40 | -1.00 | 3.50 |
| R | 0.784(7) | 0.799(3) | 0.790(11) | 0.791(1) | 0.784(7) | 0.786(9) | 0.783(6) | 0.781(8) |
| M/(M+D) | 0.837 | 0.781 | 0.768 | 0.944 | 0.900 | 0.889 | 0.861 | 0.886 |
| EF s.s. | 97.54 | 92.22 | 92.73 | 133.00 | 92.49 | 132.82 | 119.15 | 117.43 |

* Ideal content based on ca. $30H_2O$ pfu.

E%={Al-[(Na+K)+2(Mg+Ca+Sr+Ba+$Fe^{2+}$)]}/[(Na+K)+2(Mg+Ca+Sr+Ba+ $Fe^{2+}$)] (Passaglia, 1970);

R=Si/(Si+Al); M=Na+K; D=ΣCa+Mg+Mn.

0.22 μm. Erionite fibres, recovered on the filters, were rinsed with ultrapure deionised water to remove residues of the incubation solution and air-dried. Then, these fibres (20 mg) were incubated for 1 h in a 150 mM KCl solution (40 mL) at neutral pH and a temperature of 37±1 °C. This solution was used to mimic, although in a simplified way, the saline content of the intra-cellular fluid (cytosol), being potassium by far its principal cation (Rowe, 2007). Incubation time in the KCl solution was set to 1 h based on the kinetics of both erionite cation exchange process and early cytotoxicity mechanism (Eborn and Aust, 1995; Ballirano et al., 2015; Pacella et al., 2021; Di Giuseppe et al., 2022).

Fibres previously treated in MGS were also incubated up to 24 hours, under the same experimental condition described above, in a 150 mM KCl solution with the addition of Ca ions (100 μM $CaCl_2$) to evaluate possible uptake of cytosolic $Ca^{2+}$ by erionite. In addition, control experiments were carried out by suspending pristine erionite fibres in ultrapure deionized water and in 100 μM $CaCl_2$ solution. For each experiment a blank procedure was always carried out. Data reported are the mean values of at least duplicate measurements (corrected considering data from the blank procedure).

#### ICP-OES investigation

One $cm^3$ of each filtered solution was properly diluted with a 1% nitric acid solution and analysed by ICP-OES to measure the concentration of leached Si, Al, Mg, Na, Ca, K, and Fe from the fibres. All measurements were performed using a Perkin–Elmer Optima 2000 DV ICP-OES spectrometer (Perkin-Elmer, USA) equipped with a glass cyclonic spray chamber. Notably, it was not possible to distinguish any minor variations in the release of Na and K from fibres in MGS and KCl solutions respectively, due to their high content in the corresponding solutions.

ICP Aristar (BDH) standard solutions in nitric acid for Si (10.000 mg $dm^{-3}$), Mg, Na, Ca, K, Fe and Al (1000 mg $dm^{-3}$) were used to make up the calibrating solutions for ICP-OES analyses. The standard solutions used for the calibration curves were made up as the samples using the MGS and KCl solution, properly diluted with a 1% nitric acid solution. To ensure adequate quality assurance, the measures of the standard solutions were regularly repeated after the measurements of each single experiment. Data reported are the average values of measurements done at least in duplicate (corrected for the corresponding blank).

#### SEM-EDS

The chemical composition of the fibres was determined using a SEM ZEISS DSM 940A equipped with a standardized LINK EDS system. Analytical conditions were: 15 kV accelerating voltage and 3.4 μA beam current. The following standards were used: wollastonite (Si Kα, Ca Kα), corundum (Al Kα), magnetite (Fe Kα), periclase (Mg Kα), orthoclase (K Kα), and jadeite (Na Kα). The final crystal chemical formulae were calculated, after renormalization of the chemical analyses assuming a water content of 18.5 wt% (corresponding to ca. 30 atoms per formula unit, apfu), based on 36 (Si+Al) apfu. Both the balance error formula E% (Passaglia, 1970) and the K content test (Cametti et al., 2013) were used for selecting the positive analyses.

#### XRPD

X-ray Powder Diffraction (XRPD) data were measured in transmission mode, θ/θ geometry, using a Bruker AXS D8 Advance. The instrument is fitted with incident beam focusing (Göbel) mirrors and a position sensitive detector (PSD) VÅntec-1. Samples were loaded in 0.6 mm diameter borosilicate glass capillaries. Diffraction patterns were measured in the 6-145 °2θ angular range, 0.022 °2θ step-size and 8 s counting time. Preliminary analysis of the data confirmed that samples contain, a part of erionite, minor chabazite and quartz plus clay minerals (possibly nontronite: Matassa et al., 2015). Quantitative phase analysis (QPA) and erionite structure refinements were performed by a mixed Pawley-Rietveld method, successfully adopted for similar samples (Pacella et al., 2017, 2021), using Topas V6 (Bruker AXS, 2016). The Fundamental Parameters Approach (Cheary and Coelho, 1992) was adopted to describe the peak shape. Starting structural data of the various phases were as follow: erionite-K (Pacella et al., 2017), chabazite (Passaglia and Ferro, 2002), and quartz (Le Page and Donnay, 1976). Because of the unavailability of a suitable structural model for nontronite, its minor contribution to the pattern was approximated by using single peaks located at the relevant $2\theta$ values of ca. 19.8, 26.9, 34.7, 55.8, 61.6, 67.7 °$2\theta$, consistent with a hexagonal $a$=5.16 Å $c$=14.8 Å lattice, observed in the different plots of the Rietveld refinements. Based on relative peaks intensity, we estimate a content of nontronite <5 wt%. Fractional coordinates and site occupancies of both extra-framework (EF) cations and $H_2O$ molecule sites were refined for erionite. Cell parameters were refined for both erionite and chabazite. An anisotropic broadening model was used to describe the peak shape of erionite to keep into account its fibrous morphology (Stephens, 1999). Absorption correction was performed using the equation of Sabine et al. (1998) for a cylindrical sample and preferred orientation was corrected using spherical harmonics (8th-order, six refinable parameters) by selecting the number of appropriate terms as suggested by Ballirano (2003). CIF files of the pristine and cation-exchanged samples are available for download at the journal site.

## RESULTS AND DISCUSSION

ICP-OES analysis of MGS after fibre incubation (Figure 2) shows a preferential release of K [12013(586) mg/kg] and Ca [9549(181) mg/kg] and a minor release of Mg [1137(26) mg/kg] from the fibres, in perfect agreement with results obtained by Pacella et al. (2021). In addition, Si and Al are leached from the fibres in a considerably lower amount than extra-framework cations [117(14) mg/kg for Si and Al below detection limit. i.e., <0.050 mg/L]. Notably, Fe release was below the detection limit (<0.050 mg/L), as expected in the adopted experimental conditions (neutral pH and presence of air).

ICP-OES analysis of 150 mM KCl solution after 1 h of sample incubation (Figure 3) shows that erionite released a considerable amount of Na [22913(48) mg/kg] and minor Ca [635(0) mg/kg] and Mg [355(1) mg/kg], indicating a possible exchange of these cations with K ions. Besides, erionite showed a similar trend of extra-framework cation release when incubated up to 24 h in KCl solution in presence of Ca ions (100 µM $CaCl_2$) (Figure 4). In particular, we observed a net Ca increase in the solution, therefore ruling out possible Ca binding by the fibres.

It should be noted that the fibres did not bind Ca even when incubated in MGS in presence of 100 µM $CaCl_2$ (Figure S1 in supporting material). Conversely, when the fibres were suspended in 100 µM $CaCl_2$ for up to 24 hours, it was observed that nearly all available Ca in the solution was acquired by erionite (Table 2). Control experiments of $CaCl_2$ solution without fibres showed no change in Ca concentration throughout the entire experimental time. In addition, incubation of erionite in water under the same experimental conditions highlighted no release of Ca (Table 2). The samples immersed in the 100 µM $CaCl_2$ solution showed an increased release of Na and K over time as compared to that observed in water and, therefore, a charge balance was calculated using the approach of Ballirano et al. (2015). The results indicated that the number of acquired charges was roughly comparable to the number of released charges (Table 2) suggesting that erionite bound Ca through cation exchange. It must be pointed out that the small discrepancies observed between released and acquired charges may be attributed to the contribution of accessory phases (i.e., nontronite and chabazite) to the leaching of cations.

The chemical analyses of the fibres after suspension in the MGS confirmed that extra-framework cations K and

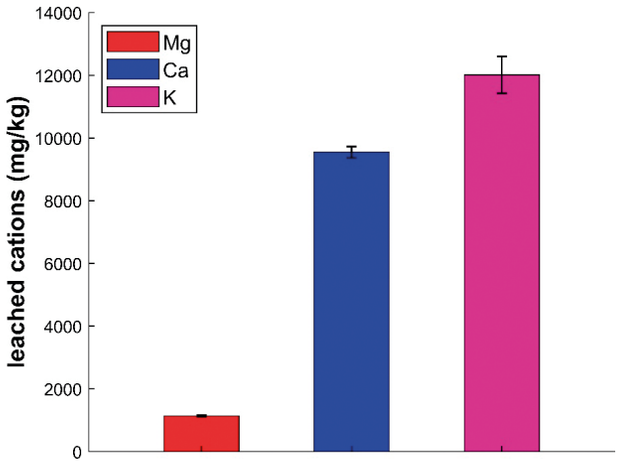


Figure 2. Cation release of erionite fibres in MGS solution at neutral pH for 24 h: release of K, Ca, and Mg extra-framework cations.

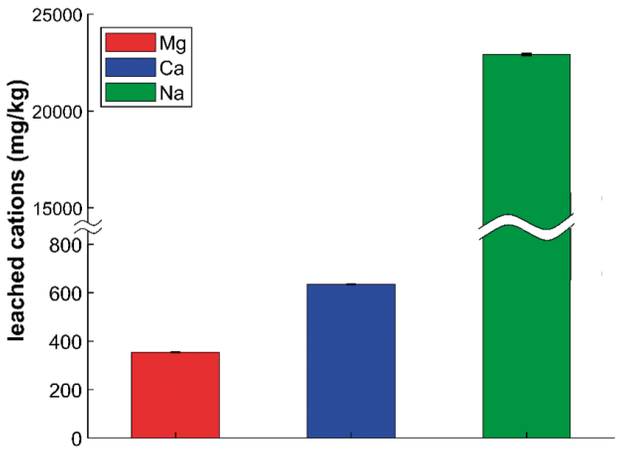


Figure 3. Cation release of erionite fibres in KCl solution at neutral pH for 1 h: release of Na, Ca, and Mg extra-framework cations.

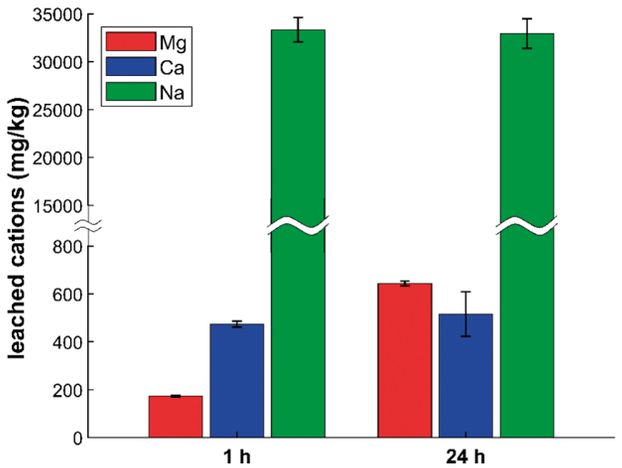


Figure 4. Cation release of erionite fibres in KCl in presence of 100 µM CaCl2 for 1 h and 24 h: release of Na, Ca, and Mg extra-framework cations.

Table 2. ICP analysis of the supernatant for extra framework cation release in ultrapure deionized water and in 100 μM $CaCl_2$ solution for 1 and 24 hours. Charge released from and acquired by erionite fibres during binding of calcium ale also reported. Standard deviations in brackets.

| | 1 hour | | 24 hours | |
|---|---|---|---|---|
| Cation release (nmol/mg) | $H_2O$ | 100 μM $CaCl_2$ | $H_2O$ | 100 μM $CaCl_2$ |
| Mg | - | 3(0) | - | 5(1) |
| Na | 77(8) | 531(79) | 84(9) | 540(1) |
| K | 7(0) | 51(10) | 7(1) | 56(1) |
| Net charge released | | | | |
| Mg | | 6(0) | | 10(2) |
| Na | | 454(87) | | 456(10) |
| K | | 44(10) | | 49(2) |
| Total | | 504(97) | | 515(14) |
| Acquired charge ($Ca^{2+}$) | | 406(27) | | 407(4) |

Ca are exchanged with Na (Table 1).

SEM-EDS results on samples incubated in KCl solution highlighted that K ions are bound by erionite fibres. In particular, the retrieved crystal chemical formula indicated a marked increase in K content, from ca. 2 to 6 apfu in the sample incubated in the MGS (starting sample) and in the KCl solution, respectively. This increased K content is counterbalanced by a significant decrease in Na content, from ca. 4 to below 0.5 apfu (Table 1), which aligns perfectly with the ICP-OES data.

The final average crystal-chemical formula obtained was $(Na_{0.35}K_{6.17}Mg_{0.58}Ca_{0.24})[Al_{7.71}Si_{28.29}O_{72.22}]\cdot 30.62H_2O$. Notably, the K content is comparable to that measured on fibres incubated up to 2 hours in KCl by Pacella et al. (2017) despite differences in the experimental conditions (4M KCl and a solid-liquid ratio of 10:1) (Table 1). The same trend was observed when comparing the EDS analysis of fibres incubated in KCl solution with the addition of $Ca^{2+}$ ions (100 μM $CaCl_2$), even if the amount of K bound to erionite at the expense of Na is slightly lower (ca. 5 apfu, see Table 1). It is important to point out that for both these samples no increase in Ca content was highlighted compared to the starting material (ERI-Gamble 24 h, see Table 1). This finding is in perfect agreement with the ICP-OES results and further supports that erionite is unable to bind $Ca^{2+}$ ions under the adopted experimental conditions.

Quantitative Phase Analysis (QPA) testifies a relevant homogeneity of the samples as the chabazite and quartz content is very constant (Table 3). The structural data (Tables 4 and 5) clearly depict the path of the various exchange processes. Ca3 site is the first one to deplete whereas Ca1 undergoes a partial (in MGS) or complete (K-exchange) reduction of its s.s.. K release occurring during leaching in MGS produces a decrease of s.s. at K2, conversely permanence in KCl solutions causes a

Table 3. QPA of the various samples. Clays were observed in all samples but were not quantified owing to the absence of an adequate structural model (see text). The content has been estimated to be similar in all samples and <5 wt% from visual evaluation of the intensity of the relevant reflections.

| Leaching time | ERI-PRI | ERI-KCl Ref 2h | ERI-KCl 1h | ERI-KCl+$CaCl_2$ 1h | ERI-KCl+$CaCl_2$ 24h | ERI-Gamble 24h |
|---|---|---|---|---|---|---|
| Erionite | 96.42(13) | 97.15(8) | 95.40(17) | 95.21(15) | 95.85(18) | 95.59(17) |
| Chabazite | 3.50(13) | 2.75(8) | 4.55(17) | 4.74(15) | 4.10(18) | 4.35(17) |
| Quartz | 0.07(1) | 0.10(1) | 0.05(1) | 0.05(1) | 0.05(1) | 0.07(1) |
| Clays | > | > | > | > | > | > |

Table 4. Miscellaneous data of the Rietveld refinements including agreement indices, cell parameters of erionite and coexisting chabazite, site scattering (s.s.) at both extra framework (EF) and $H_2O$ sites. Statistical indicators as defined in Young (1993). *Originally not reported by the authors.

| Leaching time | ERI-PRI | ERI-KCl Ref 2 h | ERI-KCl 1 h | ERI-KCl+$CaCl_2$ 1 h | ERI-KCl+$CaCl_2$ 24 h | ERI-Gamble 24 h |
|---|---|---|---|---|---|---|
| $R_{wp}$ | 1.73 | 1.81 | 2.00 | 2.09 | 2.06 | 1.90 |
| $R_p$ | 1.30 | 1.31 | 1.50 | 1.55 | 1.54 | 1.43 |
| $\chi^2$ | 3.12 | 4.04 | 3.28 | 3.23 | 3.37 | 3.32 |
| DWd | 0.33 | 0.21 | 0.32 | 0.31 | 0.30 | 0.32 |
| $R_{Bragg}$ erionite | 0.44 | 0.65 | 0.62 | 0.67 | 0.66 | 0.50 |
| Cell parameters chabazite | | | | | | |
| *a* (Å) | 9.3761(5) | 9.3796(5)* | 9.3793(3) | 9.3788(3) | 9.3794(4) | 9.3696(5) |
| *a* (Å) | 94.450(6) | 94.530(6)* | 94.542(4) | 94.546(4) | 94.548(5) | 94.376(6) |
| V (Å$^3$) | 816.41(12) | 817.03(13)* | 816.90(7) | 816.76(8) | 816.90(10) | 814.96(13) |
| Cell parameters erionite | | | | | | |
| *a* (Å) | 13.23178(8) | 13.22555(8) | 13.22581(8) | 13.22536(8) | 13.22585(8) | 13.22577(8) |
| *C* (Å) | 15.06458(8) | 15.07846(10) | 15.07659(8) | 15.07636(8) | 15.07671(8) | 15.07601(8) |
| c/a | 1.13851(1) | 1.14001(1) | 1.13994(1) | 1.13996(1) | 1.13994(1) | 1.13990(1) |
| V (Å$^3$) | 2284.15(3) | 2284.10(3) | 2283.91(3) | 2283.72(3) | 2283.94(3) | 2283.80(3) |
| EF site scattering s.s. ($e^-$) | | | | | | |
| Ca1 | 18.6(6) | - | - | - | - | 9.0(6) |
| Ca2 | 30.9(3) | 26.1(8) | 29.3(4) | 29.9(4) | 29.4(4) | 33.9(3) |
| Ca3 | 9.3(7) | 5.3(5) | 0.4(4) | 0.9(4) | 0.4(4) | 0.0(4) |
| K1 | 38.0(0) | 38.0(0) | 38.0(0) | 38.0(0) | 38.0(0) | 38.0(0) |
| K2 | 13.9(5) | 24.7(7) | 21.3(7) | 19.2(7) | 23.2(7) | 10.2(5) |
| Total cat. s.s. refinement | 110.7(21) | 94.1(20) | 89.0(15) | 88.0(15) | 91.0(15) | 91.1(18) |
| Total cat. s.s. from SEM-EDS | 97.5 | 133.0 | 132.8 | - | - | 88.6 |
| $H_2O$ sites s.s. ($e^-$) | | | | | | |
| OW7 | 21.3(15) | 45.2(7) | 45.4(7) | 47.0(6) | 45.9(10) | 31.4(7) |
| OW8 | 44.3(4) | 37.9(7) | 40.6(5) | 41.0(5) | 40.9(5) | 31.9(5) |
| OW9 | 47.5(11) | 49.7(15) | 51.9(21) | 51.0(22) | 55.6(30) | 44.8(10) |
| OW10 | 47.8(16) | 23.3(9) | 25.1(11) | 22.1(11) | 20.0(14) | 48.8(10) |
| OW11 | 39.6(15) | 54.3(19) | 49.5(26) | 52.7(27) | 49.8(35) | 45.8(13) |
| OW12 | 55.2(11) | 71.7(9) | 73.7(9) | 75.2(9) | 73.9(9) | 61.5(13) |
| Total s.s. $H_2O$ sites | 255.7(72) | 282.1(66) | 286.2(79) | 289.0(80) | 286.1(103) | 264.3(57) |
| $H_2O$ pfu | 32.0(9) | 35.3(8) | 35.8(10) | 36.1(10) | 35.8(12) | 33.0(7) |
| Total cat.+ $H_2O$ sites s.s. refinement | 366(9) | 376(9) | 375(9) | 377(10) | 377(12) | 355(7) |
| Total cat.+ $H_2O$ sites s.s. from SEM-EDS | 335 | 379 | 375 | | | 324 |

Table 5. *z* coordinates of Ca1 and Ca2 cation sites; individual and average T-O bond distances; Al population at T1 [Al(1)] and T2 [Al(2)] tetrahedral sites as calculated from the Jones' determinative curves (Jones, 1968) $Al_{pop}$=6.4116 *x*<T-O> - 10.282. Tabulated values were multiplied by the site multiplicity (T1=24; T2=12).

| Leaching time | ERI-K | ERI-KCl Ref 2 h | ERI-KCl 1 h | ERI-KCl+$CaCl_2$ 1 h | ERI-KCl+$CaCl_2$ 24 h | ERI-Gamble 24 h |
|---|---|---|---|---|---|---|
| z Ca1 | 0.887(2) | - | - | - | - | 0.873(3) |
| z Ca2 | 0.0988(6) | 0.1021(12) | 0.1004(7) | 0.0996(7) | 0.1004(7) | 0.0983(6) |
| z Ca3 | 0.699(4) | 0.700(5) | ¾ | ¾ | ¾ | ¾ |
| T1-O2 | 1.6391(15) | 1.6412(13) | 1.6434(14) | 1.6444(14) | 1.6431(14) | 1.6434(15) |
| T1-O4 | 1.6295(12) | 1.6369(12) | 1.6363(13) | 1.6378(11) | 1.6363(12) | 1.6263(11) |
| T1-O1 | 1.616(3) | 1.606(3) | 1.602(3) | 1.602(3) | 1.605(3) | 1.621(3) |
| T1-O3 | 1.634(2) | 1.625(2) | 1.626(2) | 1.624(2) | 1.625(2) | 1.637(2) |
| <T1-O> | 1.630 | 1.627 | 1.627 | 1.628 | 1.627 | 1.632 |
| T2-O6 | 1.615(2) | 1.616(2) | 1.606(3) | 1.605(2) | 1.607(3) | 1.623(2) |
| T2-O1 | 1.657(2) | 1.667(2) | 1.667(2) | 1.666(2) | 1.663(2) | 1.646(2) |
| T2-O1 | 1.657(2) | 1.667(2) | 1.667(2) | 1.666(2) | 1.663(2) | 1.646(2) |
| T2-O5 | 1.651(3) | 1.634(2) | 1.633(2) | 1.633(2) | 1.633(2) | 1.654(2) |
| <T2-O> | 1.645 | 1.646 | 1.643 | 1.643 | 1.642 | 1.642 |
| Al(1) apfu | 4.05 | 3.65 | 3.59 | 3.75 | 3.65 | 4.35 |
| Al(2) apfu | 3.18 | 3.27 | 3.03 | 3.03 | 2.91 | 2.97 |
| $Al_{tot}$ apfu | 7.23 | 6.92 | 6.62 | 6.78 | 6.56 | 7.32 |
| $Si_{tot}$ apfu | 28.77 | 29.08 | 29.38 | 29.22 | 29.44 | 28.68 |
| R=Si/(Si+Al) | 0.799 | 0.808 | 0.816 | 0.812 | 0.818 | 0.797 |
| R from SEM-EDS | 0.782(6) | 0.791 | 0.786(9) | - | - | 0.790(6) |

significant increase, as previously described (Pacella et al., 2017). Only very minor differences are observed among the samples incubated in KCl and KCl+$CaCl_2$ solutions. A very peculiar behavior has been observed: both pristine and incubated in MGS samples show a total s.s. at the cation sites calculated from the refinement higher than that arising from SEM-EDS analysis. In the case of the K-exchanged samples the behavior is reversed. We will return on this aspect below.

As far as the population of the $H_2O$ sites is referred to, immersion in MGS causes generalized modifications of the various occupancies. The most relevant ones are the significant transfer of s.s. from OW8 to OW7 and the overall moderate increase of the total s.s. at the various $H_2O$ sites with respect to the pristine sample [264(6) vs 256(7) $e^-$]. As in the case of the cation sites, only marginal differences were observed among the samples kept in KCl and KCl+$CaCl_2$ solutions at different times. The modifications of s.s., with respect to the pristine sample, at the various $H_2O$ sites are significant but without noticeable displacement of their positions. The most important is the major increase at OW7 and OW12 and the corresponding relevant decrease at OW10. The overall increase of the total s.s. at the various $H_2O$ sites is significantly higher than that observed in the case of the sample incubated in MGS, in agreement with the same pattern previously observed by Pacella et al. (2017).

Moreover, the sum of the s.s. at the cation and $H_2O$ sites almost perfectly match that arising from SEM-EDS analysis in the case of the K-exchanged samples whereas it is significantly higher (ca. 30 $e^-$) for the sample (relatively Na-rich) immersed in MGS.

Those results suggest the following points:

a) A relevant fraction of the EF cations is allocated at or near $H_2O$ sites in agreement with the results of Pacella et al. (2017).

b) The SEM-EDS microchemical data underestimate the Na content owing to alkali metal migration (Pacella et al., 2016).

c) Points a) and b) cannot be attributed to the assumption

made of a content of ca. 30 $H_2O$ pfu as, in the case of the K-exchanged samples, the refined sum of the s.s. at the cation and $H_2O$ sites almost perfectly match that obtained from SEM-EDS.

d) There are no detectable structural differences among the various samples incubated in KCl and KCl in presence of $Ca^{2+}$ ions (100μM $CaCl_2$).

The XRPD data collection for the sample kept for 24 h in a KCl+100 μM $CaCl_2$ solution was repeated after 3 months of curing at RT of the capillary to check the potential existence of a kinetic ordering of the EF cations allocated at or near $H_2O$ sites. No structural differences, at the 1s level, were observed.

Chabazite cell parameters change as a function of the leaching environment. In the case of the incubation in KCl-rich solutions both the *a*-parameter and the *α* angle increase, as compared to the pristine sample [9.3761(5) Å and 94.450(6)], in a remarkably constant way (Table 4). In fact, the average over the three samples (KCl and KCl+100 μM $CaCl_2$ for 1 and 24 h) is of 9.3792(4) Å and 94.545(5)°. The cell parameters agree with those measured by Pacella et al. (2017) and originally not reported in the paper (Table 4) for the sample of erionite-Na incubated for 2 h in a KCl solution. Leaching in the MGS produces a decrease of both the *a*-parameter and the *α* angle [9.3696(5) Å and 94.376(6)°, respectively]. The unit-cell modifications testify that chabazite undertakes some cation exchange and therefore provides a minor contribution to the release of ions into solution because of its limited abundance in the mixture (ca. 4 wt%).

Comparison of the present data with those reported by Ballirano and Cametti (2015) for incubation in Gamble's solution of erionite-Na is very difficult. In fact, the chemistry of pristine erionite was different (Ca-free) with respect to that of the material used in this work. This is due to the fact that erionite from Rome, Oregon is characterized by a relatively large chemical variability and in the same hand specimen patches showing different composition are commonly observed. Moreover, the Gamble's solution also included acetate and citrate, as well as additional Ca and K salts, according to the formulation of Marques et al. (2011) with respect to the present simplified composition.

## CONCLUSIONS

Recently, it has been suggested that erionite fibres are too short to undergo frustrated phagocytosis, resulting in a limited role of phagocytosis in the acute toxicity of these fibres (Di Giuseppe et al., 2022). Alternatively, it has been inferred that fibrous erionite, when in contact with the cell medium, undergoes a cation exchange process with ions dispersed in the extracellular fluids (mainly $Na^+$) and, after phagocytosis, with cytoplasmic ions (e.g., $Ca^{2+}$ and $K^+$). Consequently, erionite fibres engulfed by macrophage cells can lead to the release of substantial amounts of $Na^+$ into the cytosol, disrupting ion homeostasis and causing cell injury (Di Giuseppe et al., 2022). Our results partially support this hypothesis, showing that erionite can bind K when immersed in a solution mimicking intra-cellular K concentration, following a rapid cation exchange with the extra-framework cations, mainly Na. Moreover, an internal redistribution of extra-framework cations occurs within the erionite cage, resulting in an increase in electron density at K2 site where adsorbed $K^+$ ions are allocated. However, our results ruled out possible uptake of Ca ions by erionite when immersed in a KCl solution at cytosolic concentration. This indicates that cytosolic $Ca^{2+}$ is hardly fixed by erionite fibres within their structure and, on this basis, the fibres should not lead to the failure of cell apoptosis by interfering with the cross-talk between endoplasmic reticulum and mitochondria. To confirm these findings on the possible mechanism of erionite's acute toxicity, ongoing research is dedicated to examining the crystal-chemical modifications of the fibres following their interaction in a real cellular environment (THP-1 macrophages).

### ACKNOWLEDGEMENTS

We would like to thank the two anonymous reviewers whose comments and suggestions helped to improve our manuscript. This research was conducted earlier under project "Fibres: a multidisciplinary mineralogical, crystal-chemical and biological project to amend the paradigm of toxicity and cancerogenicity of mineral fibres" (PRIN – Bando 2017 - Prot. 20173 × 8WA4).

## REFERENCES

Artvinli M. and Baris Y.I., 1979. Malignant mesotheliomas in a small village in the Anatolian region of Turkey: an epidemiologic study. Journal of the National Cancer Institute 63, 17-22.

Ballirano P., 2003. Effects of the choice of different ionization level for scattering curves and correction for small preferred orientation in Rietveld refinement: The $MgAl_2O_4$ test case. Journal of Applied Crystallography 36, 1056-1061.

Ballirano P., Andreozzi G.B., Dogan M., Dogan A.U., 2009. Crystal structure and iron topochemistry of erionite-K from Rome, Oregon, USA. American Mineralogist 94, 1262-1270.

Ballirano P., Bloise A., Gualtieri A.F., Lezzerini M., Pacella A., Perchiazzi N., Dogan M., Dogan A.U., 2017. The crystal structure of mineral fibres. In: A.F. Gualtieri (Ed.) "Mineral fibres: crystal chemistry, chemical-physical properties, biological interaction and toxicity". European Mineralogical Union, London, 17-64.

Ballirano P., Pacella A., Cremisini C., Nardi E., Fantauzzi M., Atzei D., Rossi A., Cametti G., 2015. Fe (II) segregation at a specific crystallographic site of fibrous erionite: A first step toward the understanding of the mechanisms inducing its

carcinogenicity. Microporous and Mesoporous Materials 211, 49-63.

Ballirano P. and Cametti G., 2012. Dehydration dynamics and thermal stability of erionite-K: Experimental evidence of the "internal ionic exchange" mechanism. Microporous and Mesoporous Materials 163, 160-168.

Ballirano P. and Cametti G., 2015. Minerals in the human body. Crystal chemical and structural modifications of erionite fibers leached with simulated lung fluids. American Mineralogist 100, 103-112.

Baris Y.I., Artvinli M., Saracci R., Simonato L., Pooley F., Skidmore J., Wagner C., 1987. Epidemiological and environmental evidence of the health effects of exposure to erionite fibres: a four-year study in the Cappadocian region of Turkey. International Journal of Cancer 39, 10-17.

Baris Y.I., Simonato L., Saracci R., Skidmore J.W., Artvinli M., 1981. Malignant mesothelioma and radiological chest abnormalities in two villages in central Turkey: An epidemiological and environmental investigation. The Lancet, 317(8227), 984-987.

Bruker AXS, 2016. Topas V6: General profile and structure analysis software for powder diffraction data. Bruker AXS, Karlsruhe, Germany.

Cametti G., Pacella A., Mura F., Rossi M., Ballirano P., 2013. New morphological, chemical, and structural data of woolly erionite-Na from Durkee, Oregon, U.S.A. American Mineralogist 98, 2155-2163.

Cangiotti M., Salucci S., Battistelli M., Falcieri E., Mattioli M., Giordani M., Ottaviani M.F., 2018. EPR, TEM and cell viability study of asbestiform zeolite fibers in cell media. Colloids and Surfaces B: Biointerfaces 161, 147-155.

Carbone M., Baris Y.I., Bertino P., Brass B., Comertpay S., Dogan A.U., ... Miller A., 2011. Erionite exposure in North Dakota and Turkish villages with mesothelioma. Proceedings of the National Academy of Sciences 108, 13618-13623.

Cheary R.W. and Coelho A., 1992. Fundamental parameters approach to x-ray line-profile fitting. Journal of Applied Crystallography 25, 109-121.

Coffin D.L., Cook P.M., Creason J.P., 1992. Relative mesothelioma induction in rats by mineral fibers: comparison with residual pulmonary mineral fiber number and epidemiology. Inhalation Toxicology 4, 273-300.

Coombs D.S., Alberti A., Armbruster T., Artioli G., Colella C., Galli E., ... Vezzalini G., 1998. Recommended nomenclature for zeolite minerals: report of the subcommittee on zeolites of the International Mineralogical Association, Commission on New Minerals and Mineral Names. Mineralogical Magazine 62, 533-571.

Di Giuseppe D., Scarfì S., Alessandrini A., Bassi A.M., Mirata S., Almonti V., … Gualtieri A.F., 2022. Acute cytotoxicity of mineral fibres observed by time-lapse video microscopy. Toxicology 466, 153081.

Eborn S.K. and Aust A.E., 1995. Effect of iron acquisition on induction of DNA single-strand breaks by erionite, a carcinogenic mineral fiber. Archives of Biochemistry and Biophysics 316, 507-514.

Gard J.A. and Tait J.M., 1973. Refinement of the crystal structure of erionite. In Proceedings of the Third International Conference on Molecular Sieves, 94-99.

Gottardi G. and Galli E.,1985. Natural Zeolites. Minerals and Rocks 18.

Gualtieri A.F., Gandolfi N.B, Pollastri S., Pollok K., Langenhorst F., 2016. Where is iron in erionite? A multidisciplinary study of fibrous erionite-Na from Jersey (Nevada, USA). Scientific Reports 6, 37981.

Gualtieri A.F., Gandolfi N.B, Pollastri S., Burghammer M., Tibaldi E., Belpoggi F., Draži´c G., 2017. New insights into the toxicity of mineral fibres: A combined in situ synchrotron μ-XRD and HR-TEM study of chrysotile, crocidolite, and erionite fibres found in the tissues of Sprague-Dawley rats. Toxicology Letters 274, 20-30.

Ilgren E.B., Kazemain H., Hoskins J.A., 2015. Kandovan the next 'Capadoccia'? A potential public health issue for erionite related mesothelioma risk. Epidemiology, Biostatistics, and Public Health 12.

Ilgren E.B., Pooley F.D., Larragoitia J.C., Talamantes M., Navarrete G.L., Krauss E., Breña A.F., 2008. First confirmed erionite related mesothelioma in North America. Indoor Built Environ 17, 567-568.

International Agency for Research on Cancer (IARC), 2012. In Arsenic, metals, fibres, and dusts Vol. 100C Monographs on the evaluation of carcinogenic risks to humans, 219-309.

Le Page Y. and Donnay G., 1976. Refinement of the crystal structure of low-quartz. Acta Crystallographica B32, 2456-2459.

Matassa R., Familiari G., Relucenti M., Battaglione E., Downing C., Pacella A., ... Ballirano P., 2015. A deep look into erionite fibres: An electron microscopy investigation of their self-assembly. Scientific reports 5, 16757.

Marques M.R.C., Loebenberg R., Almukainzi M., 2011. Simulated biological fluids with possible application in dissolution testing. Dissolution Technologies 18, 15-28.

Ortega-Guerrero M.A., Carrasco-Núñez G., Barragán-Campos H., Ortega M.R., 2015. High incidence of lung cancer and malignant mesothelioma linked to erionite fibre exposure in a rural community in Central Mexico. Occupational and Environmental Medicine 72, 216-218.

Pacella A., Ballirano P., Cametti G., 2016. Quantitative chemical analysis of erionite fibres using a micro-analytical SEM-EDX method. European Journal of Mineralogy 28, 257-264.

Pacella A., Ballirano P., Fantauzzi M., Rossi A., Viti C., Arrizza L., Nardi E., Caprioli R., Montereali M.R., 2021. Surface and bulk modifications of fibrous erionite in mimicked Gamble's solution at acidic pH. Minerals 11, 914.

Pacella A., Cremisini C., Nardi E., Montereali M.R., Pettiti I., Ballirano P., 2017. The mechanism of iron binding processes

in erionite fibres. Scientific reports 7, 1319.
Passaglia E., 1970. The crystal chemistry of chabazites. American Mineralogist 55, 1278-1301.
Passaglia E. and Ferro O., 2002. Occurrence and crystal structure of magnesian chabazite. In Studies in Surface Science and Catalysis 142, 1729-1735.
Pollastri S., Gualtieri A.F., Vigliaturo R., Ignatyev K., Strafella E., Pugnaloni A., Croce A., 2016. Stability of mineral fibres in contact with human cell cultures. An in situ μXANES, μXRD and XRF iron mapping study. Chemosphere 164, 547-557.
Rom W.N., Casey K.R., Parry W.T., Mjaatvedt C.H., Moatamed F., 1983. Health implications of natural fibrous zeolites for the Intermountain West. Environmental Research 30, 1-8.
Rowe N., 2007. Fluid Balance and Management and the Critically Ill Woman. In book: Critical Care in Childbearing for Midwives. Publisher: BlackwellEditors: Mary Billington, Mandy Stevenson.
Sabine T.M., Hunter B.A., Sabine W.R., Ball C.J., 1998. Analytical expressions for the transmission factor and peak shift in absorbing cylindrical specimens. Journal of Applied Crystallography 31, 47-51.
Staples L. and Gard J., 1959. The fibrous zeolite erionite; its occurrence, unit cell, and structure. Mineralogical Magazine and Journal of the Mineralogical Society 32(247), 261-281.
Stephens P.W., 1999. Phenomenological model of anisotropic peak broadening in powder diffraction. Journal of Applied Crystallography 32, 281-289.